Effect of Zr/Hf ratio on ionic conductivity of $(Zr_xHf_{1-x}O_2)_{0.9}(Y_2O_3)_{0.1}$ ceramics

Susumu Nakayama (Department of Applied Chemistry and Biotechnology, National Institute of Technology (KOSEN), Niihama College, s.nakayama@niihama-nct.ac.jp, Japan)

Abstract

Yttria- and scandia-stabilized zirconia are pivotal in solid-state oxide fuel cell research owing to their exceptional oxide ion conduction properties. In addition, the similarity between Hf and Zr, combined with their abundance, underscores the significance of exploring yttria-stabilized hafnia as a potential alternative. In this study, we aim to enhance our understanding of the properties and potential applications of such materials in sustainable energy technologies. Thus, the effect of the Zr/Hf ratio on the oxide ionic conductivities of $(Zr_xHf_{1-x}O_2)_{0.9}(Y_2O_3)_{0.1}$ compounds is investigated by varying the Zr/Hf ratio in the range of 1.00/0.00/0.00/1.00. We determined that the oxide ionic conductivity intragrain decreases with increasing Hf contents, and the apparent activation energy with respect to the oxide ionic conduction increases. The standard enthalpy of formation per one oxygen atom is –572.35 and –550.28 kJ mol^{-1} for Hf-O and Zr-O, respectively. In addition, it is confirmed that the Hf-O bond is stronger than the Zr-O bond. Therefore, it is assumed that oxide ion conduction does not occur easily when Hf atoms are adjacent to oxide ions.

Key words

impedance analyzer, Nyquist plot, Arrhenius plot, XRD, SEM-EDX

1. Introduction

Yttria-stabilized zirconia [$(ZrO_2)_{0.92}(Y_2O_3)_{0.08}$, 8YSZ], which exhibits high oxide ion conduction, has remained the most extensively studied electrolyte material for solid-state oxide fuel cells; it is recognized as the most efficient of all fuel cells (Nakayama et al., 2021). However, there are also many reported cases of scandia-stabilized zirconia [$(ZrO_2)_{0.89}(Sc_2O_3)_{0.10}(CeO_2)_{0.01}$, 10Sc1CeSZ] that exhibit even higher oxide ion conductions. SOFCs using 8YSZ and 10Sc1CeSZ as electrolytes have already been commercialized (Nakayama et al., 2021; Nakayama, 2023).

Hf and Zr belong to the same group of elements and exhibit very similar chemical and physical properties because of their similar valences and atomic and ionic radii. The atomic and ionic radii of Zr and Hf are the same for the following reasons. In the periodic table, Hf occupies the sixth period, one period after Zr, which occupies the fifth period. However, the effect of the increase in atomic and ionic radii owing to the increase in period is cancelled by the "lanthanide contraction" phenomenon of the lanthanide series, which occurs immediately before Hf. Hf is found in the Earth's crust at a concentration of approximately 3.3 ppm, where it commonly coexists with Zr in Zr-bearing minerals. Considerable research has been conducted on yttria-stabilized hafnia in which Zr is replaced by Hf in yttria-stabilized zirconia (Alotaibi et al., 2021; Johansen and Cleary, 1964; Sevin et al, 2020; Trubelje and Stubican, 1991). However, although there are reported cases of Zr and Hf alone, there are few reports of systems with systematically different Zr/Hf ratios (Bonnet et al, 2021; Yu et al., 2023). Yu et al. (2023) studied the hardness, fracture toughness, and thermal conductivity of yttrium partially stabilized zirconia/hafnia $(Zr_{1-x}Hf_xO_2)_{0.97}(Y_2O_3)_{0.03}$ (x = 0.00, 0.25, 0.50, 0.75, and 1.00) at room temperature.

In this study, we investigated the change in the ionic conductivity of cubic yttria-stabilized zirconia/hafnia ceramics $[(Zr_{1-x}Hf_xO_2)_{0.9}(Y_2O_3)_{0.1}]$ when the Zr/Hf ratio is varied over a wide range.

2. Experimental procedure

EP grade zirconium oxide (ZrO_2) was purchased from Daiichi Kigenso Kagaku Kogyo Co., Ltd. Hafnium oxide (HfO_2) with a purity of 98 % was obtained from Kojundo Chemical Laboratorary Co., Ltd. 3N grade yttrium oxide (Y_2O_3) was purchased from Shin-Etsu Chemical Co., Ltd. ZrO_2, HfO_2, and Y_2O_3 were blended to the prescribed composition and wet-mixed for 3 h in a planetary ball mill using a zirconia container and balls. After drying at 100 °C, the mixture was packed in an alumina (Al_2O_3) crucible (SSA-S, Nikkato Co.) and temporarily calcined at 1200 °C for 2 h. After drying at 100 °C, the obtained temporarily sintered material was wet-crushed in a planetary ball mill for 2 h. After drying at 100 °C, the material was formed into a disk of diameter 13 mm by a 100-MPa die press and sintered for 2 h in an electric furnace at 1600 °C on an Al_2O_3 setter covered with electro-fused zirconia coarse powder. The sintering process was performed in an electric furnace at 1600 °C for 2 h.

The surface crystalline phase of the sintered samples was determined by X-ray diffraction (XRD, Rigaku Co., MiniFlex II) of the sintered surface in the 2θ range of 20-80° using the $CuK_{\alpha 1}$ line. The surface structures of the sintered samples were observed by scanning electron microscopy (SEM, JSM-6510LA, JEOL Co.) and analyzed by field-emission scanning

electron microscopy (FE-SEM, JSM-7500F, JEOL Ltd.) with energy-dispersive X-ray spectroscopy (EDX, JEOL Ltd., JED-2300). The samples for electrical measurements were prepared as follows. After coating both sides of each sintered sample (diameter (φ), 10 mm × thickness (t), 1 mm) with a Pt paste (Pt electrode; φ = 6 mm, t = 1 mm) and attaching a Pt wire (φ = 0.05 mm), the sample was baked (1000 °C). The Pt wire attached to the sample was wound around a Pt main wire (φ = 0.5 mm) and connected for the measurements. Conductivity measurements of the samples were performed in the temperature range 300-500 °C using an impedance meter (HP4194A) in the frequency range of 100 Hz to 10 MHz. The ionic conductivities were determined by complex impedance analyses.

3. Results and discussion

XRD patterns of the sintered surfaces of the $(Zr_{1-x}Hf_xO_2)_{0.9}(Y_2O_3)_{0.1}$ (x = 0.00, 0.25, 0.50, 0.75, and 1.00) ceramics are shown in Figure 1. Regardless of the x value, only peaks attributable to cubic crystals were observed for all samples. The crystal structures of pure ZrO_2 and HfO_2 are monoclinic, tetragonal, or cubic. The monoclinic phase is stable at room temperature. The tetragonal and cubic phases, which are stable at high temperatures, are also stable at room temperature when ZrO_2 and HfO_2 are solid-dissolved with Y_2O_3. When monoclinic phases are present, monoclinic (-111) and (111) peaks (reported in ICCD No. 37-1484) are observed at 2θ = 28° and 31°, respectively, on both sides of the cubic (111) peak, which is observed at 2θ = 30°. When tetragonal phases are present, (321) and (114) peaks (reported in ICCD No. 17-923) are observed at 2θ = 69° and 77°, respectively, on both sides of the cubic (400) peak, which is observed at 2θ = 74°. However, no peaks attributed to the monoclinic or tetragonal phases are observed in the $(Zr_{1-x}Hf_xO_2)_{0.9}(Y_2O_3)_{0.1}$ (x = 0.00, 0.25, 0.50, 0.75, and 1.00) ceramics.

SEM images of the surfaces of the $(Zr_{1-x}Hf_xO_2)_{0.9}(Y_2O_3)_{0.1}$ (x = 0.00, 0.25, 0.50, 0.75, and 1.00) ceramics are shown in Figure 2. The crystal grain sizes at x = 0.00, 0.25, 0.50, 0.75, and 1.00 are approximately 5.0, 3.0, 4.0, 2.5, and 2.0 μm, respectively. The greater the Hf content (x values), the smaller the grain size. The reflected electron image and the EDX profile of the surface of the $(Zr_{1-x}Hf_xO_2)_{0.9}(Y_2O_3)_{0.1}$ (x = 0.50) ceramic (Figure 3) show that the atomic percentages of Zr, Hf, and Y in each grain are nearly equal. Therefore, the abundance of Zr, Hf, and Y is considered to be constant in each grain. Based on these results, a microstructure is proposed for the $(Zr_{1-x}Hf_xO_2)_{0.9}(Y_2O_3)_{0.1}$ ceramics, which is composed of intergrains, grain boundaries, and voids, as shown in Figure 4.

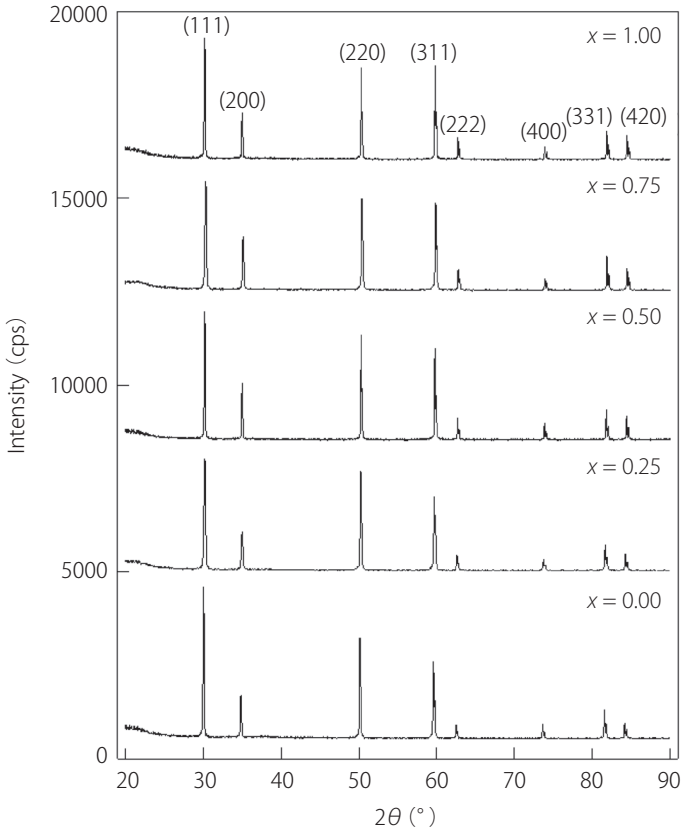

Figure 1: XRD patterns of the sintered surface on the $(Zr_{1-x}Hf_xO_2)_{0.9}(Y_2O_3)_{0.1}$ ceramics (x = 0.00, 0.25, 0.50, 0.75, and 1.00)

Note: The numbers represent the miller indexes of cubic ZrO_2 reported in ICDD No. 27-997.

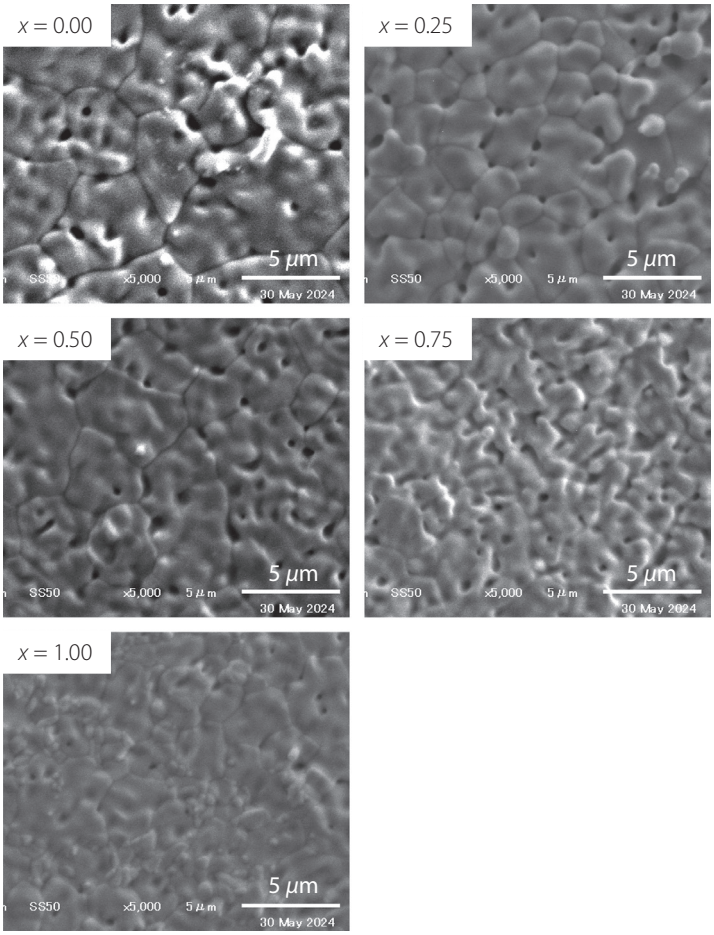

Figure 2: SEM images of the sintered surface on $(Zr_{1-x}Hf_xO_2)_{0.9}(Y_2O_3)_{0.1}$ ceramics (x = 0.00, 0.25, 0.50, 0.75, and 1.00)

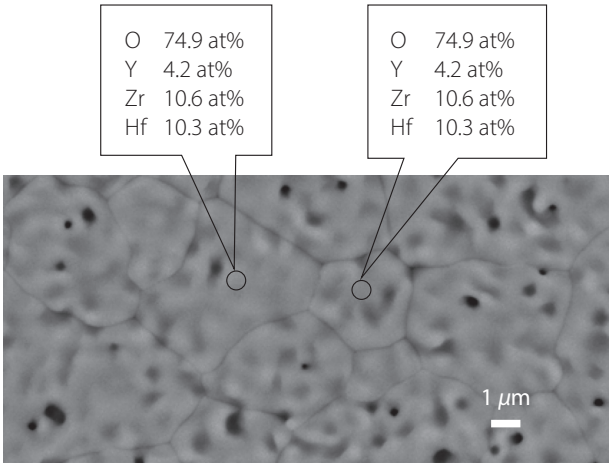

Figure 3: Reflected electron image of the sintered surface on the $(Zr_{1-x}Hf_xO_2)_{0.9}(Y_2O_3)_{0.1}$ ceramics (x = 0.50) and point analysis data obtained by energy-dispersive X-ray spectroscopy

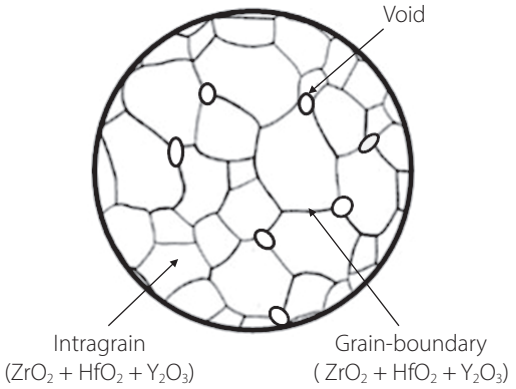

Figure 4: Proposed microstructure of $(Zr_{1-x}Hf_xO_2)_{0.9}(Y_2O_3)_{0.1}$ ceramics

Figures 5 and 6 show Nyquist plots of $(Zr_{1-x}Hf_xO_2)_{0.9}(Y_2O_{3)0.1}$ (x = 0.00, 0.50, and 1.00) at 300 and 500 °C, respectively. Intragranular (R_b), grain-boundary (R_{gb}), and electrode interface resistances hinder ionic conduction in ceramics. In the Nyquist plot for x = 0.00 (Figure 2), arcs caused by the R_b and R_{gb} within the ceramics were observed. Moreover, in the Nyquist plot at 500 °C for x = 0.00 in Figure 3, arcs caused by the R_{gb} and electrode interface resistance between ceramics and the Pt electrode were observed. Among these resistance components, we focused on the R_b, which was considered less susceptible to various factors (e.g., grain boundaries and the amount of voids that affect porosity) during ceramic fabrication. Furthermore, it was confirmed by EDX analysis that Zr, Hf, and Y were present uniformly in the R_b being evaluated. We also believe that the difference in the grain size of ap-

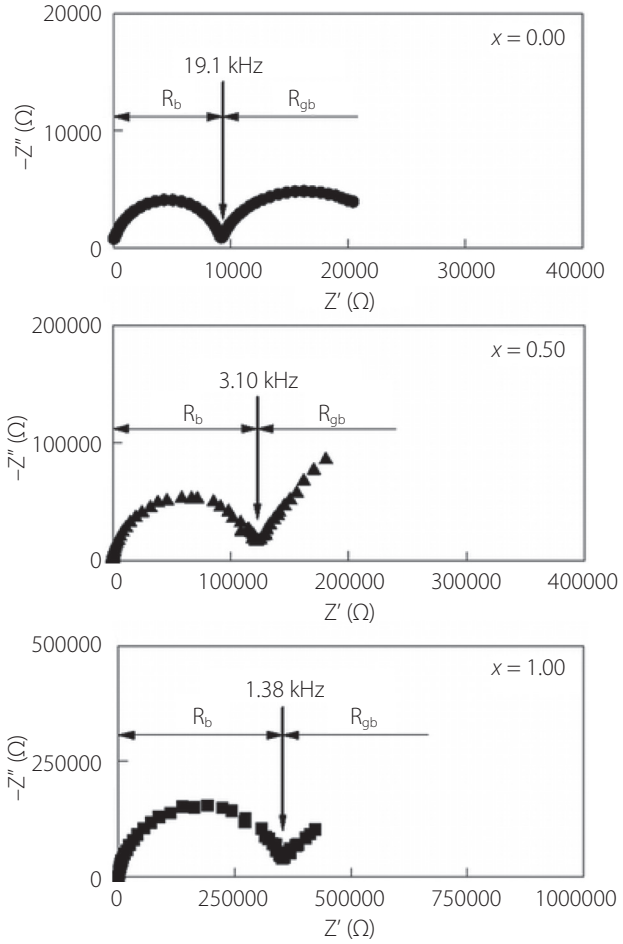

Figure 5: Nyquist plots of $(Zr_{1-x}Hf_xO_2)_{0.9}(Y_2O_3)_{0.1}$ ceramics (x = 0.00, 0.50, and 1.00) at 300 °C

Note: R_b and R_{gb} refer to the intragranular and grain-boundary resistances in ceramics, respectively.

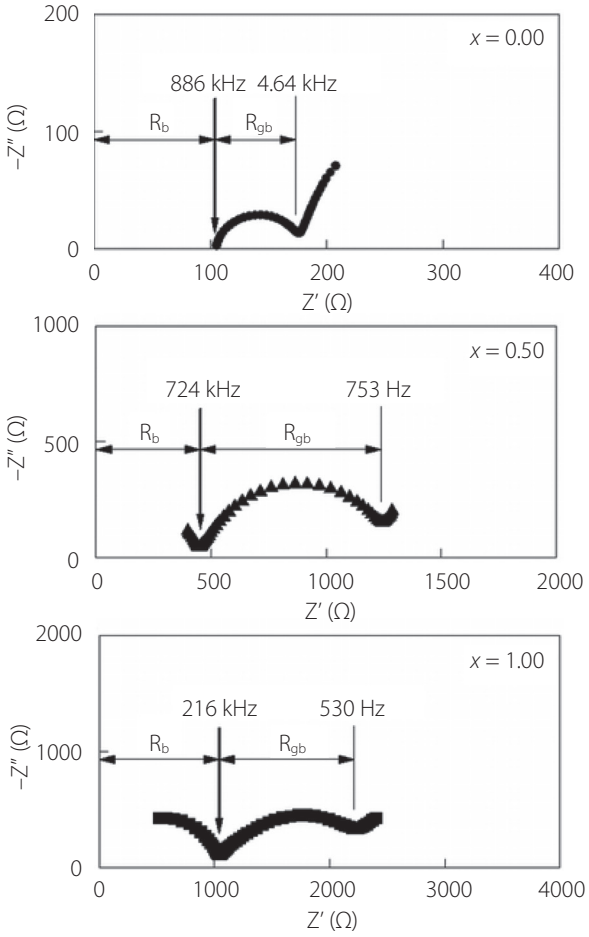

Figure 6: Nyquist plots of $(Zr_{1-x}Hf_xO_2)_{0.9}(Y_2O_3)_{0.1}$ ceramics (x = 0.00, 0.50, and 1.00) at 500 °C

proximately 2.0 to 5.0 μm has little effect on R_b. The R_b was obtained from the Z′-axis values of the dashed arrows in each Nyquist plot.

The conductivities of the R_b components of the $(Zr_{1-x}Hf_xO_2)_{0.9}(Y_2O_3)_{0.1}$ ceramics were parameterized using the Arrhenius equation:

$$\sigma T = \sigma_0 \cdot \exp(-E/kT),$$

where σ, σ_0, E, k, and T are the conductivity, pre-exponential factor, activation energy, Boltzmann constant, and absolute temperature, respectively. The intragrain oxide ion conductivities of the $(Zr_{1-x}Hf_xO_2)_{0.9}(Y_2O_3)_{0.1}$ (x = 0.00, 0.25, 0.50, 0.75, and 1.00) ceramics at 300, 350, 400, 450, and 500 °C, which were determined using Arrhenius plots, are summarized in Figure 7. The apparent activation energies of ionic conductions of the $(Zr_{1-x}Hf_xO_2)_{0.9}(Y_2O_3)_{0.1}$ ceramics were determined from the slopes of the Arrhenius plots. The oxide ion conductivity of the $(Zr_{1-x}Hf_xO_2)_{0.9}(Y_2O_3)_{0.1}$ ceramics tended to decrease with increasing Hf contents (x values). The apparent activation

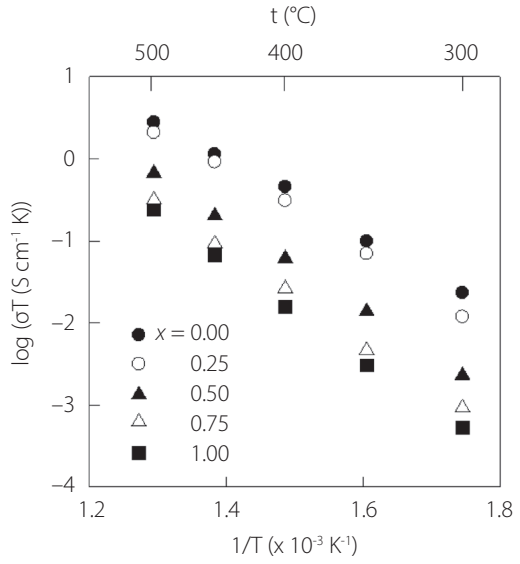

Figure 7: Arrhenius plots of the conductivities in the grains of $(Zr_{1-x}Hf_xO_2)_{0.9}(Y_2O_3)_{0.1}$ ceramics (x = 0.00, 0.25, 0.50, 0.75, and 1.00)

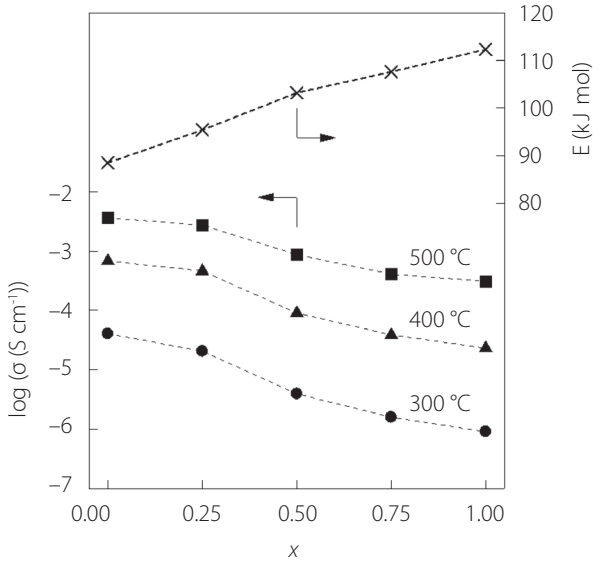

Figure 8: Relationship between the Hf content (*x* values) of $(Zr_{1-x}Hf_xO_2)_{0.9}(Y_2O_3)_{0.1}$ ceramics and the conductivities in the grains at 300, 400, and 500 °C, and the apparent activation energies for the ionic conductivities in the grains

energy for ionic conduction was obtained from the slope of the Arrhenius plot. The relationship between the *x* composition of the ceramics and apparent activation energy for oxide ion conduction is shown in Figure 8. Similarly, the figure shows the relationship between the *x* values of the $(Zr_{1-x}Hf_xO_2)_{0.9}(Y_2O_3)_{0.1}$ ceramics and oxide ion conductivities at 300, 400, and 500 °C. The ionic conductivity tended to decrease with increasing x values, although it was not linearly proportional, which assisted oxide ion migration. Sevin et al. (2020) reported that the intragrain and grain-boundary oxide ion conductivities of $(ZrO_2)_{0.92}(Y_2O_3)_{0.08}$ ceramics at 300 and 500 °C were 1.5×10^{-5} and 1.0×10^{-3} S cm^{-1}, respectively, and those of $(HfO_2)_{0.79}(Y_2O_3)_{0.11}$ ceramics at 300 and 500 °C were 3.0×10^{-7} and 1.0×10^{-4} S cm^{-1}. Although the amount of stabilizer Y_2O_3 differed from this study, and the oxide ion conductivities of the intragrain and combined intragrain and grain-boundary resistances differed, the order of magnitude and size relationship in the ion conductivities were similar.

As shown in Figure 9 (a), in pure ZrO_2 and HfO_2, oxide ions were regularly arranged, and there was no space for the oxide ions to move. In other words, achieving oxide ion conduction was difficult. However, in yttria-stabilized zirconia/hafnia, in which tetravalent Zr and Hf were partially replaced by trivalent Y, oxygen vacancies formed, as shown in Figure 9 (b). Oxide ions were partially missing from the electrical neutrality condition. The oxygen vacancies allowed the oxide ions to move, as indicated by the arrows in the figure. It was hypothesized that the higher *x*-values in the $(Zr_{1-x}Hf_xO_2)_{0.9}(Y_2O_3)_{0.1}$ ceramics influenced the ease with which oxide ions migrated. Although the cubic $(Zr_{1-x}Hf_xO_2)_{0.9}(Y_2O_3)_{0.1}$ ceramics and crystal

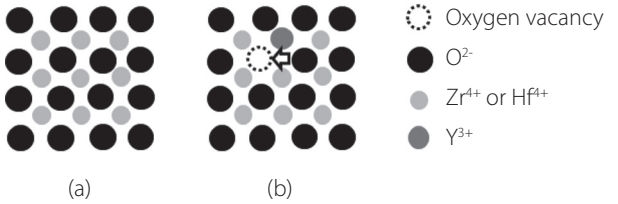

Figure 9: (a) Schematic diagram of the ideal ZrO_2 and HfO_2 crystal structures, and (b) atomic arrangement and ion conduction mechanism of ZrO_2 and HfO_2 without oxide ions owing to the Y^{3+} substitution of Zr^{4+} and Hf^{4+}

systems differed, the standard enthalpies of formation for monoclinic ZrO_2 and HfO_2 were –1100.56 and –1144.7 kJ mol^{-1}, respectively (the Chemical Society of Japan, 1993). The lower the standard enthalpy of formation per oxygen atom, the stronger was the bond between the metal elements. The standard enthalpies of formation per one oxygen atom for Hf-O and Zr-O were –572.35 and –550.28 kJ mol^{-1}, respectively. The oxide ions of the ion-conducting species were considered to be more bound and less mobile when Hf was adjacent compared with when Zr was adjacent, because the standard enthalpy of formation per oxygen atom was lower, which complicates the migration process.

4. Conclusion

$(Zr_{1-x}Hf_xO_2)_{0.9}(Y_2O_3)_{0.1}$ (x = 0.00, 0.25, 0.50, 0.75, 1.00) ceramics were prepared, and the *x* values and oxide ionic conductivities were investigated. From these results, it was concluded that $(Zr_{1-x}Hf_xO_2)_{0.9}(Y_2O_3)_{0.1}$ tended to decrease as the *x* value increased. However, there was not a linearly proportional relationship between the *x* value and oxide ionic conductivity intragrain. The apparent activation energy for the ionic conduction from the slope of the Arrhenius plot for the oxide ionic conductions of the $(Zr_{1-x}Hf_xO_2)_{0.9}(Y_2O_3)_{0.1}$ ceramics showed a tendency to increase with increasing x values.

Acknowledgement

We would like to thank Daiichi Kigenso Kagaku Kogyo Co., Ltd. for supplying us with EP and Editage (www.editage.jp) for English language editing.

References

Alotaibi, M., Li, L., and West, A.R. (2021). Electrical properties of yttria-stabilised hafnia ceramics. *Physical Chemistry Chemical Physics*, Vol. 23, 25951-25960.

Bonnet, E., Grenier, J. C., Bassat, J. M., Jacob, A., Delatouche, B., and Bourdais, S. (2021). On the ionic conductivity of some zirconia-derived high-entropy oxides. *Journal of the European Ceramic Society*, Vol. 41, 4505-4515.

Chemical Society of Japan (ed.) (1993). *Handbook of chemistry: Pure chemistry, 4th ed.*, II-288, 294.

Johansen, H. A. and Cleary, J. G. (1964). High-temperature electrical conductivity in the systems CaO-ZrO_2 and CaO-HfO_2. *Journal of the Electrochemical Society*, Vol. 111, 100-103.

Nakayama, S., Itani, K., Yasui, T., Watanabe, S., and Mizuno, T. (2021). Relationship between SiO_2 content and electrical properties of 8-mol% Y_2O_3-stabilized ZrO_2 electrolyte. *Studies in Science and Technology*, Vol. 10, 191-196.

Nakayama, S., Tokunaga, R., Takata, M., Kondo, S., and Nakajima, Y. (2021). Crystal phase, electrical properties, and solid oxide fuel cell electrolyte application of scandia-stabilized zirconia doped with rare earth elements. *Open Ceramics*, Vol. 6, 100136.

Nakayama, S. (2023). Effect of annealing on the valence state of Ce ions and electrical properties in $(ZrO_2)_{0.88}(CeO_2)_{0.12}$ and $(ZrO_2)_{0.89}(Sc_2O_3)_{0.1}(CeO_2)_{0.01}$. *Results in Materials*, Vol. 18, 100395.

Sevin, L., Razafindramanana, V., Julian-Jankowiak, A., Justin, J-F., Mauvy, F., and Rebillat, F. (2020). Effect of high-content Yttria on the thermal expansion behaviour and ionic conductivity of a stabilised cubic Hafnia. *Journal of the European Ceramic Society*, Vol. 40, 5859-5869.

Trubelje, M. F. and Stubican, V. S. (1991). Ionic conductivity in the hafinia-R_2O_3 systems. *Solid State Ionics*, Vol. 49, 89-97.

Yu, Z., Qi, T., Ge, M., Zhang, W., Hu, Z., and Sun, X. (2023). Microstructures and phase compositions of Y_2O_3-ZrO_2-HfO_2 solid solutions. *Ceramics International*, Vol. 49, 26119-26128.

Received: May 15, 2024
Accepted: June 10, 2024
Published: June 30, 2024

https://doi.org/10.11425/sst.13.55